REPORT DOCUMENTATION PAGE

The public reporting burden for this collection of information is estimated to average 1 hour per response, including the time for reviewing instructions, searching existing data sources, gathering and maintaining the data needed, and completing and reviewing the collection of information. Send comments regarding this burden estimate or any other aspect of this collection of information, including suggestions for reducing the burden, to the Department of Defense, Executive Service Directorate (0704-0188). Respondents should be aware that notwithstanding any other provision of law, no person shall be subject to any penalty for failing to comply with a collection of information if it does not display a currently valid OMB control number.
PLEASE DO NOT RETURN YOUR FORM TO THE ABOVE ORGANIZATION.

1. REPORT DATE (DD-MM-YYYY)	2. REPORT TYPE	3. DATES COVERED (From - To)
25/07/2011	Final Performance Report	15/06/2008 - 30/11/2010

4. TITLE AND SUBTITLE
Polymeric and Molecular Materials for Advanced Organic Electronics

5a. CONTRACT NUMBER
FA9550-08-1-0331/P00001

5b. GRANT NUMBER
FA9550-08-1-0331/P00001

5c. PROGRAM ELEMENT NUMBER

6. AUTHOR(S)
Marks, Tobin J. and Facchetti, Antonio (Northwestern University)
Dodabalapur, Ananth (University of Texas at Austin)

5d. PROJECT NUMBER

5e. TASK NUMBER

5f. WORK UNIT NUMBER

7. PERFORMING ORGANIZATION NAME(S) AND ADDRESS(ES)
Dept. of Chemistry, Northwestern University, 2145 Sheridan Rd. Evanston IL 60208
Dept. of Electrical and Computer Engineering, The University of Texas at Austin10100 Burnet Rd., Bldg 160, Room 2.206E, Austin TX 78758

8. PERFORMING ORGANIZATION REPORT NUMBER

9. SPONSORING/MONITORING AGENCY NAME(S) AND ADDRESS(ES)
USAF, AFRL DUNS 143574726
AF OFFICE OF SCIENTIFIC RESEARCH
875 N. RANDOLPH ST. ROOM 3112
ARLINGTON VA 22203

10. SPONSOR/MONITOR'S ACRONYM(S)
AFOSR

11. SPONSOR/MONITOR'S REPORT NUMBER(S)
AFRL-OSR-VA-TR-2012-0269

12. DISTRIBUTION/AVAILABILITY STATEMENT
A

13. SUPPLEMENTARY NOTES

14. ABSTRACT
During the project period, we made strong progress in: 1) organic semiconductors, 2) gate dielectrics, and 3) fundamental studies of charge transport. In 1), we expanded our understanding of the architectural and electronic structure requirements for n-type semiconductors and the role grain boundaries play in transport. To accomplish this, we developed new synthetic routes to processable small molecules and polymers, and characterized/optimized structural, electronic, and processing properties. In 2), we expanded the SAND (self-assembled nanodielectric) concept to vapor-deposited (V-SAND) and to spin-coated, printable variants. All have excellent dielectric and insulating properties, a remarkable ability to minimize trapped charge between thin film transistor dielectric and semiconductor layers, and because of the high capacitances, lowered transistor operating voltages. These characteristics enable many new types of devices with outstanding performance, such as transparent and flexible transistors. In 3), we showed via variable-temperature studies that transport mechanisms involve multiple trapping and release mechanisms which are sensitive to the semiconductor film processing and the gate dielectric.

15. SUBJECT TERMS
Organic transistor, organic gate dielectric, polymer semiconductor, polymer dielectric, transparent transistor, flexible transistor

16. SECURITY CLASSIFICATION OF:			17. LIMITATION OF ABSTRACT	18. NUMBER OF PAGES	19a. NAME OF RESPONSIBLE PERSON
a. REPORT	b. ABSTRACT	c. THIS PAGE			Dr. Charles Lee (AFOSR)
				21	19b. TELEPHONE NUMBER (Include area code) 703 696 7779

Polymeric and Molecular Materials for Advanced Organic Electronics

Tobin J. Marks and Antonio Facchetti, Northwestern U.
Ananth Dodabalapur, U. Texas at Austin

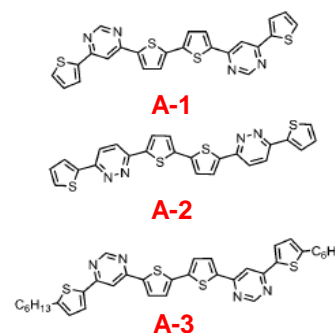t-marks@northwestern.edu, a-facchetti@northwestern.edu, ananth.dodabalapur@engr.utexas.edu

The goal of this project is to lay the groundwork for printed organic and hydbrid organic/inorganic electronics technologies by developing new solution-processable high carrier mobility semiconductors and high-*k*/high dielectric strength dielectrics. We aim to understand the critical chemical and physical phenomena affecting charge injection and transport in unconventional electronic devices as a necessary feedback for materials optimization. During this period we made substantial contributions to the following areas:

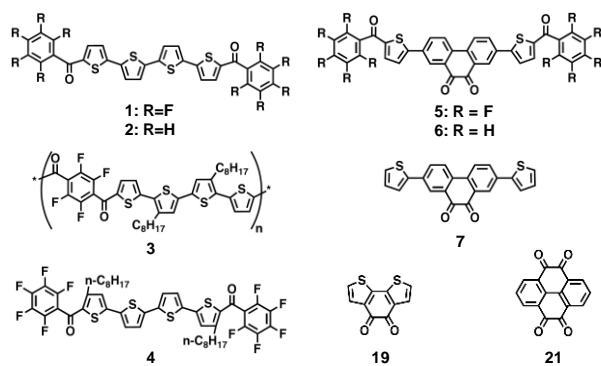## *1. Organic Semiconductor Development*

Here we summarize selected achievements in realizing new molecular and polymeric organic semiconductors for TFTs, with emphasis on key figures of merit achieved in conventional TFT architectures. This work was motivated by the fact that semiconducting materials exhibiting high mobility and current modulation in air are crucial to achieving high-speed low power consumption organic CMOS (complementary) circuits, where both p- and n-type transistors must be fabricated and integrated. In particular, we targeted the greatest challenge, n-type semiconductors, where the principal synthetic strategy followed was to "convert" established, stable, high-performance p-type cores into n-type cores, and to design completely new electron-poor π-conjugated building blocks. This results in lower HOMO and LUMO energies, the latter being the frontier MO into which the electron charge carriers are injected during transport. The outcome of these efforts was greater electron stabilization, which should induce a majority carrier "flip" from p to n (if the unsubstituted core is intrinsically hole-transporting) and enhance environmental stability (if the material is electron-transporting).

Development of New Azine-Based Semiconductors. In this synthetic task we developed new electron-depleted molecular semiconductors using azine heterocycles (pyridine, pyrazine, pyrimidine, **A1-A3**) as electron-poor cores (**Fig. 1**). Three new diazine-functionalized oligothiophenes were synthesized, and their structural, optical, vibrational spectrocopic, electrochemical, and semiconductor properties studied. Interestingly, the molecular properties of these systems are dominated by the central bithiophene (electron-rich) fragment rather than by the peripheral electron-poor units. Therefore, their properties correspond largely to π-electron extended bithiophenes. This is surprising in the case of charge mobility since, a priori, these materials would appear to be best suited for electron transport. These diazine-functionalized oligothiophenes are reasonably efficient hole

Figure 1. Chemical structures of azine-based semiconductors

transporters, typical of readily oxidized oligothiophenes. Further work will focus on modification of azine synthons, for example with electron acceptors, which should effect majority charge carrier sign inversion, or even more interestingly, afford ambipolar semiconductors able to transport both holes (owing to the bithiophene portion) and electrons (owing to the azine units).

Figure 2. Chemical structures of carbonyl-containing semiconductors.

N-type Carbonyl-Containing Oligo-/Poly-thiophenes. As discussed above, high-mobility

2

n-type organic semiconductors are essential for organic CMOS. In previous efforts, we realized the synthesis and characterization of alkylcarbonyl- and arenecarbonyl-functionalyzed (acyl) quaterthiophenes (e.g., **1,2** in **Fig. 2**) and demonstrated record electron mobilities for both vapor-deposited (~ 2 cm^2 V^{-1}s^{-1}) and solution-processed (0.25 cm^2 V^{-1}s^{-1}) devices under inert atmosphere. These results show that our n-type semiconductors have great potential, and that performance optimization should be achievable by combining with a proper gate dielectric (see below). Starting from these results, we achieved complete air-stability in this family by synthesizing quinone-based structures **5-7** (**Fig. 2**). Electronic structure computations (DFT/B3LYP/-3-21G* level) confirm that these quinone cores are planar (necessary for close molecular packing) and more electron-deficient (more negative electron affinity; lower LUMO energy) than the parent derivatives. The first crystal structure of quinone-containing thiophene-based molecule **7** reveals anti-parallel dipole alignment and cofacial packing with a short 3.48 Å π-π stacking distance. Introduction of a phenanthrenequinone unit, one of the three electron-deficient quinones identified, affords oligomer **5**, exhibit air-stable n-channel FET operation with $\mu_e \approx 0.02$ cm^{2}V^{-1}s^{-1} and a high $I_{on:off} = 10^6$ under ambient conditions. The FET performance improves with increasing deposition temperature (T_D) when measured under vacuum. When measured in air, V_T exhibits negligible change and μ_e exhibits a slight decrease in magnitude, and is then stable for greater than one year when stored and measured under laboratory air (**Fig. 3**).
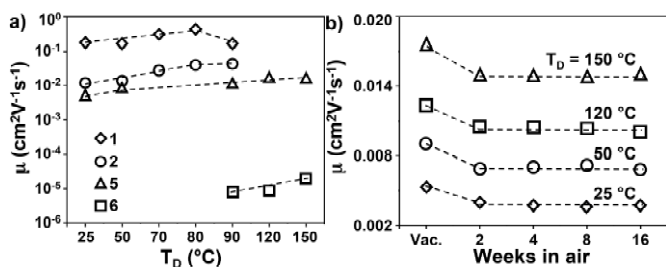
Figure 3. Plot of measured FET μ vs. T_D for oligomers **1**, **2**, **5**, and **6** (**a**) and μ_e vs. number of weeks storage in air for **5** films deposited at the indicated T_D (**b**). Dashed lines are a guide to the eye.

Cyanated Rylene Semiconductors. Core-cyanated rylenes (perylenes and naphthalenes) were discovered at Northwestern U. and are currently the best n-channel semiconductors, considering their facile synthesis, excellent electron transport, and ambient stability. Polyera Corp., a spin-off company from Northwestern U., is currently commercializing these materials. These derivatives, N,N'-difunctionalized with alkyl and fluoroalkyl groups, exhibit the highest n-type carrier mobilities in air reported to date (0.l0 - 0.80 cm^2/Vs) in combination with low threshold voltages and substantial processing versatility. Initial experiments demonstrated that solution-cast **PDI8-CN$_2$** (R = *n*-C$_8$H$_{17}$) films on SiO$_2$ exhibit electron mobilities in air > 0.2 cm^2/Vs. Electrochemistry reveals reduction potentials ~ 0.0 V vs. S.C.E.; hence electrons are greatly stabilized in the LUMOs of these molecules. The naphthalene derivatives are promising not only because of their high electron mobilities but also because of their optical transparency in the visible. Combining **NDI8-CN$_2$** (R = *n*-C$_8$H$_{17}$) with a polymeric insulator (developed at NU, see below) enabled the first "invisible" organic circuit with excellent optical transparency.

During the past project period, we continued efforts to optimize/discover new semiconductors based on rylene structures and improved the carrier mobilities of perylenes to > 1 cm^2/Vs for solution-processed devices, as well as developed an understanding, at the fundamental level, of what molecular parameters

**PDIR-CN$_2$** **NDIR-CN$_2$** **ADIR-CN$_2$**
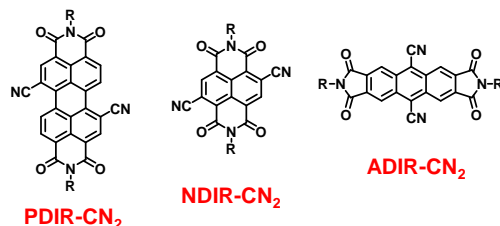
Figure 4. Molecular structures of third-generation core-cyanated rylene semiconductors.
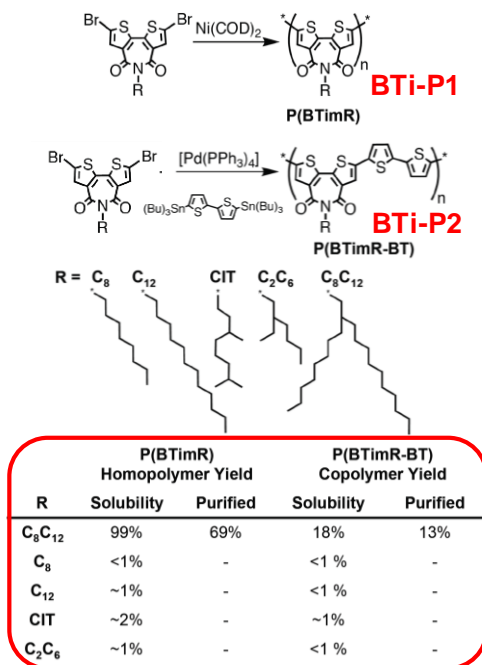
3

contribute to air stability in this unique semiconductor family. Furthermore, new rylene structures based on linear acenes (anthracene, ADIR-CN$_2$ **Fig. 4**) were synthesized and the crystal structures evidence improved packing and optimized molecular orientations on the insulator surface. Also for these new materials unoptimized electron mobilities > 0.1 cm2/Vs were demonstrated in ambient.

In addition, we explored a "soluble precursor" route approach to the perylene family, which is the first example for n-channel materials (**Fig. 5**). In this strategy, the Diels-Alder reaction of anthracene-functionalized perylenes with dienophiles was employed to synthesize the soluble precursor, which can then be converted to the active semiconductor via a retro Diels-Alder process. Soluble precursors **II** can then be converted to the corresponding semiconductors, i.e., compounds **I**, upon application of heat. This strategy is currently under investigation, however, several soluble PDI-functionalized precursos were synthesized and converted to the insoluble products in excellent yields.
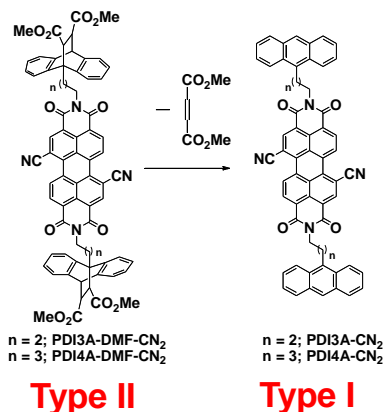
Figure 5. Chemical structures of two perylene dicarboxiimide soluble semiconductor precursors.

Polymeric Semiconductors. When we initiated this project in early 2008, electron transporting (n-channel) polymer semiconductors for TFTs were practically unknown, the few available TFTs did not operate in air, and the electron mobilities were low. One goal of this AFOSR project was to design, synthesize, and characterize new electron-deficient structures to be used as building blocks for n-channel polymers. Several new structures were developed and here we summarize only the most promising polymer families. The first is based on the *N*-alkyl-2,2'-bithiophene-3,3'-dicarboximide (BTi) core from which we have synthesized π-conjugated homopolymers and copolymers (**Fig. 6**). A novel design approach was employed using computational modeling to identify favorable **BTi** monomer properties such as core planarity, solubilizing substituent tailorability, and appropriate electron affinity. Monomeric model compounds were also synthesized to confirm these properties, and the crystal structure

R	P(BTimR) Homopolymer Yield		P(BTimR-BT) Copolymer Yield	
	Solubility	Purified	Solubility	Purified
C$_8$C$_{12}$	99%	69%	18%	13%
C$_8$	<1%	-	<1 %	-
C$_{12}$	~1%	-	<1 %	-
CIT	~2%	-	~1%	-
C$_2$C$_6$	~1%	-	<1%	-

Figure 6. Chemical structure and synthesis of various BTI homo and co-polymers where P1 and P2 are the homo- and co-polymers functionalized with a C8-C12 chain.

reveals short 3.43 Å π-π stacking distances, with favorable solubilizing substituent orientations. A family of 10 homopolymers and bithiophene copolymers was synthesized via Yamamoto and Stille polymerizations, respectively (**Fig. 6**). Two of these polymers, **BTi-P1** and **BTi-P2**, are processable in common organic solvents and exhibit n-channel and p-channel FET operation, respectively. After annealing, **BTi-P1** films exhibit a very high degree of crystallinity and an electron mobility > 0.01 cm^{2}V^{-1}s^{-1} with a current on-off ratio of 10^7, which is remarkably

independent of film-deposition conditions. Extraordinarily, **BTi-P1** films also exhibit terracing in the AFM images with a step height matching the X-ray diffraction-derived d-spacing, a rare phenomena for polymeric organic semiconductors. Another fascinating property of these materials is the air-stable p-channel FET performance of annealed **BTi-P2** films, which exhibit a hole mobility of ~0.01 $cm^2V^{-1}s^{-1}$ and a current on-off ratio of 10^7.
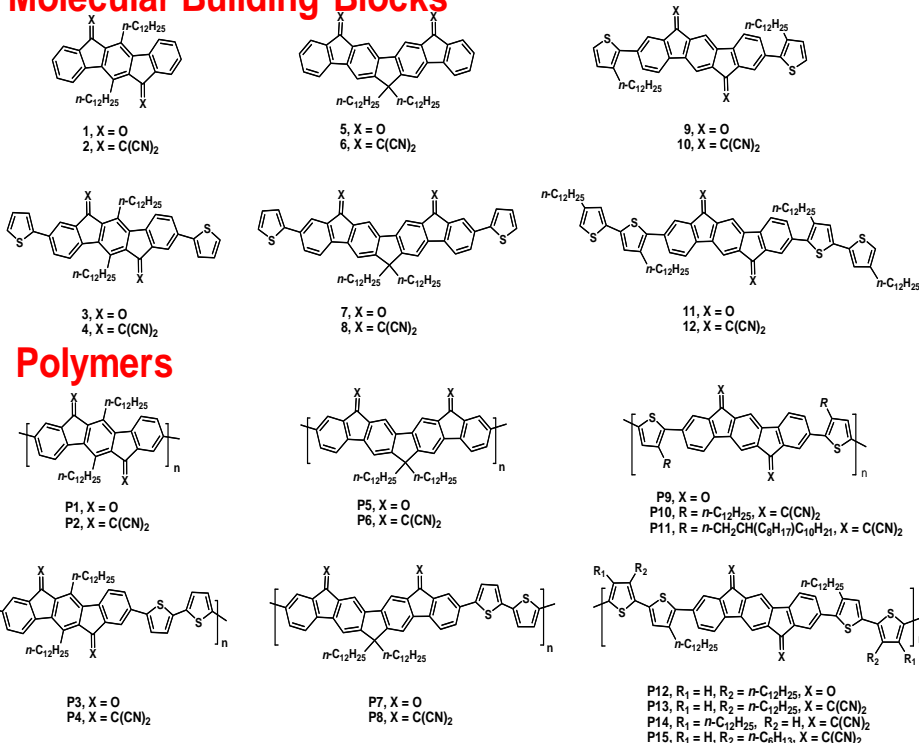
The second class of n-type semi-conductors is based on highly electron-deficient 1) indeno[1,2-b]fluorene-6,12-dione, 2,2'-(indeno[1,2-b]fluorene-6,12-diylidene) dimalononitrile, or 2) 2-bisindenofluorene-12,15-dione, and 2,2'-(bisindenofluorene-12,15-diylidene) dimalononitrile molecular building blocks (molecular structures **1 – 12** in **Fig. 7**) and their corresponding homo- and copolymers (polymer structures **P1 – P15** in **Fig. 7**). We examined in detail the effects of core size, thiophene vs. core regiochemistry, carbonyl vs. dicyanovinylene

Molecular Building Blocks

1, X = O
2, X = C(CN)$_2$

5, X = O
6, X = C(CN)$_2$

9, X = O
10, X = C(CN)$_2$

3, X = O
4, X = C(CN)$_2$

7, X = O
8, X = C(CN)$_2$

11, X = O
12, X = C(CN)$_2$

Polymers

P1, X = O
P2, X = C(CN)$_2$

P5, X = O
P6, X = C(CN)$_2$

P9, X = O
P10, R = n-C$_{12}$H$_{25}$, X = C(CN)$_2$
P11, R = n-CH$_2$CH(C$_8$H$_{17}$)C$_{10}$H$_{21}$, X = C(CN)$_2$

P3, X = O
P4, X = C(CN)$_2$

P7, X = O
P8, X = C(CN)$_2$

P12, R$_1$ = H, R$_2$ = n-C$_{12}$H$_{25}$, X = O
P13, R$_1$ = H, R$_2$ = n-C$_{12}$H$_{25}$, X = C(CN)$_2$
P14, R$_1$ = n-C$_{12}$H$_{25}$, R$_2$ = H, X = C(CN)$_2$
P15, R$_1$ = H, R$_2$ = n-C$_6$H$_{13}$, X = C(CN)$_2$

Figure 7. Chemical structures of various **BTI** homo and co-polymers where **P1** and **P2** are the homo- and co-polymers functionalized with a C8-C12 chain.
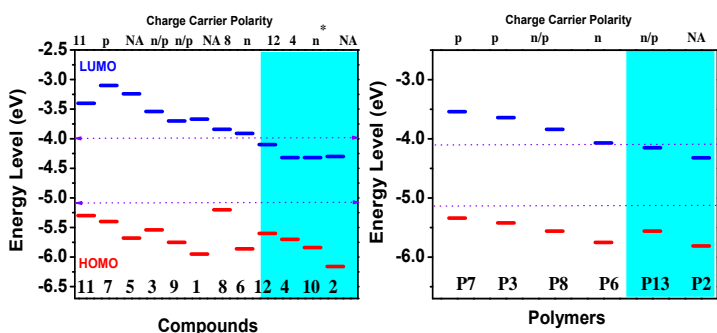
Figure 8. The energy diagram for compounds **1**-**12** (Right) and polymers **P2**, **P3**, **P6**, **P7**, **P8** , and **P13** (Left) showing experimentally estimated HOMO/LUMO energy levels and majority charge polarity.

substitution, and alkyl chain orientation on molecular properties, thin film microstructures, and OFET device performance. All of the new compounds were characterized by DSC, TGA, melting point, single-crystal X-ray diffraction (XRD), solution/thin film optical, PL, and cyclic voltammetry, to evaluate frontier MO energetics and intermolecular cohesive forces. Thin films can be grown by vacuum deposition and spin-coating, and were investigated by X-ray diffraction (XRD) and AFM. By tuning the HOMO/LUMO energetics over a 1.0 eV range, *p*-type, *n*-type, or ambipolar charge transport characteristics are observed, thus identifying the MO energetic

windows governing majority carrier polarity and air stability (**Fig. 8**). One of these systems, thiophene-terminated indenofluorenedicyanovinylene, **10**, exhibits an electron mobility of 0.16 $cm^2V^{-1}s^{-1}$ and an I_{on}/I_{off} ratio $= 10^7 - 10^8$--one of the highest to date for a solution-cast air-stable *n*-channel semiconductor film. In this family, we also discovered solution-processed ambipolar films of thiophene-based molecule **12** and copolymers **P13** and **P14**, which exhibit electron and hole mobilities of $1\times10^{-3} - 2\times10^{-4}$ and I_{on}/I_{off} ratios $\sim10^4$, representing the first examples of molecular and polymeric ambipolar semiconductors to function in air. Analysis of the operational air stabilities of a series of thin-films having different crystallinities, orientations, and morphologies suggests that operational air stability for thermodynamically-predicted (i.e., no kinetic contribution) air-stable semiconductors is principally governed by LUMO energetics, with minimal contribution from the thin film microstructure. The onset LUMO energy for carrier electron stabilization is estimated at -4.0 – -4.1 eV, indicating an overpotential of 0.9 – 1.0 eV, in line with previous stability-MO energy guidelines established for the rylene family.
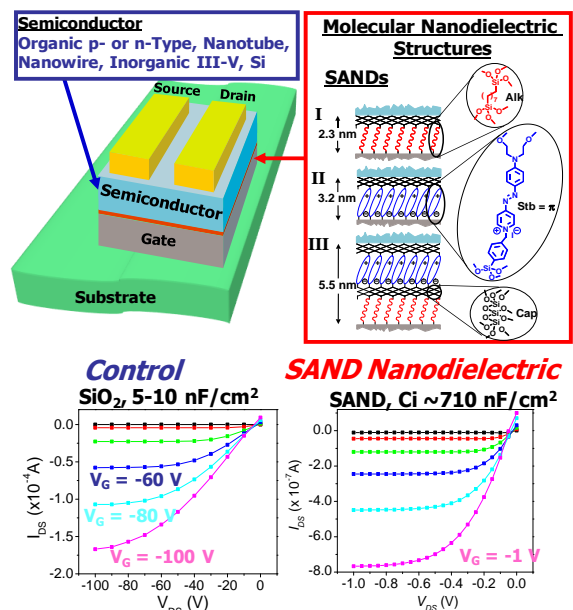
2. Gate Dielectrics for TFTs

Under this program we also developed several new classes of molecular and polymeric dielectric materials designed to enable low-voltage TFT operation, realize completely new applications, e.g, in optically transparent and nanoscopic electronics, and to be compatible with printing processes.

Molecular Insulators for Ultra-Low Voltage OTFT Operation. As noted above, the source-drain current (I_{DS}) in a TFT is proportional to the gate dielectric capacitance (C_i), which is given by (C_i) $= \varepsilon_0\ k$/d, where where *k* is the dielectric constant, ε_0 the vacuum permittivity, and *d* the dielectric thickness. For a given device geometry and semiconductor, equivalent I_{on}:I_{off} is achieved at lower operating biases by increasing C_i which stabilizes the carrier density in the semiconductor channel. In this Task, we employed self-assembly strategies to fabricate nanoscopic (small d) self-assembled multilayer dielectrics for TFTs. The first-generation of these materials utilizes 3-D crosslinked dielectrics grown from solution via self-limiting sequential deposition of chlorosilane building blocks such as α,ω-difunctionalized hydrocarbon chains (**Alk**), and highly polarizable "push-pull" π−electron stilbazolium layers (**Stb**), and Cl_3Si-O($SiCl_2$)-O-
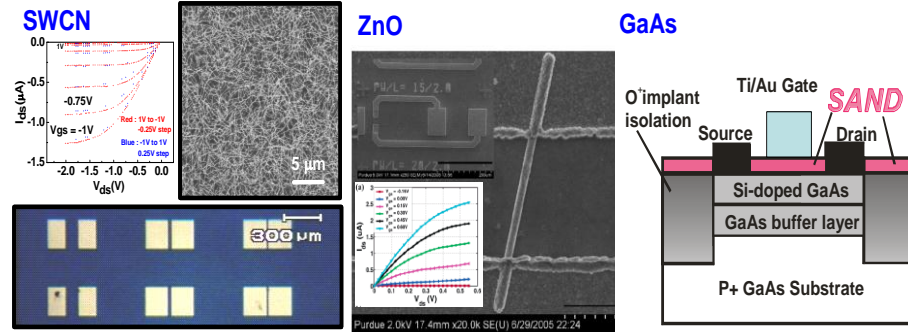

Figure 9. Top. Schematic representation of the TFT components of an OTFT based on various semiconductors and self-assembled nanodielectrics (SANDs) having structures **I-III**. Bottom. Operating voltage reduction for an oligothiophene TFT fabricated with either SiO_2 or SAND gate dielectrics.

$SiCl_3$-derived capping layers (**Cap**; **Fig. 13**). Capacitance-voltage (*C-V*) measurements on MIS structures ($10^2 - 10^5$ Hz) reveal maximum capacitances C_i = 400 (**I**); 710 (**II**); 390 (**III**) $nFcm^{-2}$ ($\pm$ 5%) at 10^2 Hz. These dielectrics find immediate applications in low-voltage organic transistors and circuits (**Fig. 9**). In addition, SAND dielectrics enable low-voltage single-walled carbon nanotube and ZnO nanowire transistors, and can be integrated with GaAs JFETs (**Fig. 9**). Because of the very large mobilities achieved in such devices ($\mu_e \sim$ 3000 $cm^2\ V^{-1}s^{-1}$ for ZnO

nanowires; $\mu_e \sim 1200$ cm^2 V^{-1}s^{-1} for single wall carbon nanotubes; $\mu_e \sim 1900$ cm^2 V^{-1}s^{-1} for GaAs;), SANDs should find application in high-speed unconventional electronics (**Fig. 10**) as well as in optically-transparent circuits and displays.

Figure 10. SAND heterogeneous integration with single wall carbon nanotubes (SWCNT network), ZnO nanowires (single wires), and GaAs transistors (wafers).
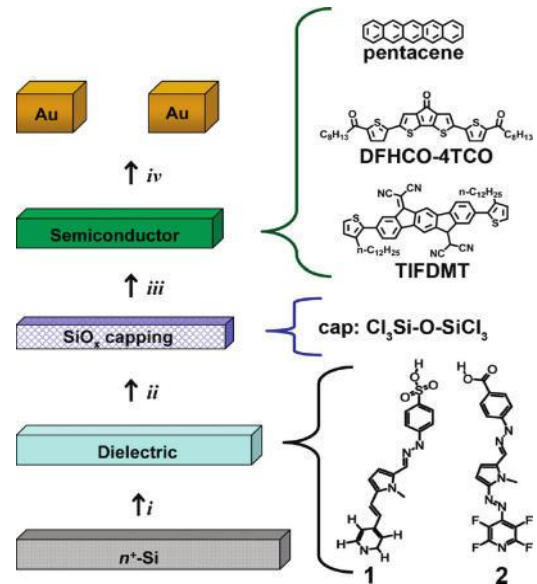
In a second approach, we recently reported under this program that TFTs could be fabricated using a solvent-free vapor-deposited self-assembled nano-dielectric (V-SAND, **Fig. 11**). These nanoscopic self-assembled gate dielectrics are structurally organized via molecular precursor hydrogen-bonding interactions, followed by planarization with a thin chemical vapor-deposited inorganic SiOx film. We showed that the metal−insulator−semiconductor (MIS) and TFT device electrical properties are sensitive to the V-SAND molecular structure and dipolar orientation. For p-type pentacene TFTs, very large mobilities (3 cm^2 V^{-1}s^{-1}) were obtained. For n-type v-SAND-based OTFTs, the performance (under vacuum and ambient) is comparable to, or surpasses, that of previously reported devices using conventional SiO$_2$ as the gate dielectric. More importantly, the devices fabricated here operate at far lower voltages. These results provide key molecular and thin-film structural information on how to design better thin dielectric films using solution-processable or vapor-phase self-assembled materials.
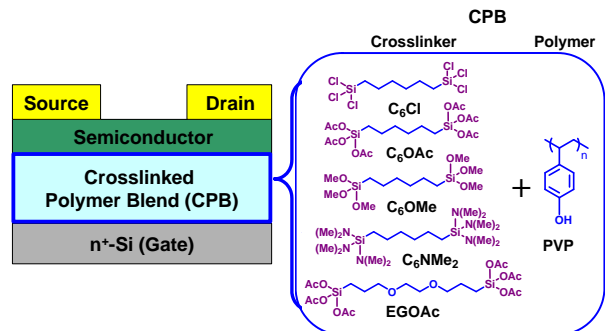

Figure 11. OFET fabrication using V-SAND as the gate dielectric via the following steps: (i) vapor deposition of molecules **1** or **2**, (ii) exposure of **F1** or **F2** to Cl$_3$SiOSiCl$_3$ vapor, completing the V-SAND structure, (iii) vapor deposition of either pentacene, **DFHCO-4TCO**, or **TIFDMT**, and (iv) vapor deposition of Au source and drain electrodes through a shadow mask.
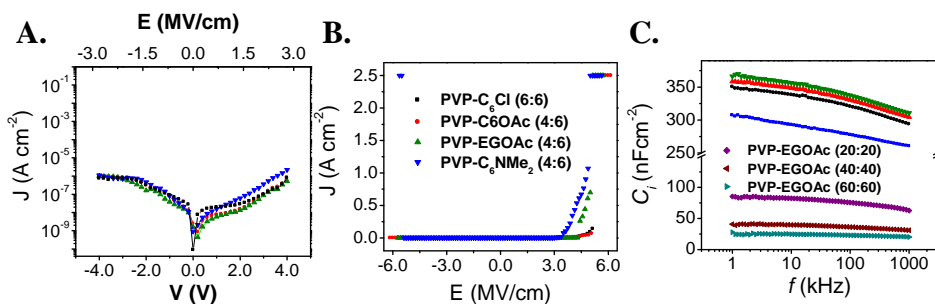
Polymeric Crosslinkable Dielectrics. There are three major limitations to current-generation polymer TFTs. The first is that, with few exceptions, they function at very large operating voltages, reflecting the intrinsically low field-effect mobilities compared to crystalline inorganic semi-conductors. Second, very few polymeric dielectrics perform optimally with both hole- and electron-transporting organic semiconductors, limiting organic CMOS

Figure 12. TFT architecture and structures of the CPB precursors (polymer and silane crosslinkers, right) used in the first-generation (C6Cl) and second-generation (the remaining) CPB dielectric materials.

7

possibilities. Third, it is very difficult with the same polymer formulation to realize printed dielectric films in high yields which exhibit large capacitances but have minimal gate leakage current at useful gate fields. In a previous investigation, we demonstrated that blending appropriate π-electron polymers, e.g., PVP, with α,ω–chlorosilane crosslinking reagents (e,g,, C_6Cl in **Fig. 12**) affords robust, adherent, pinhole-free, high-capacitance, low-leakage, ultrathin (10-20 nm) gate dielectric films. However, due to high reactivity of the chlorosilane crosslinking reagents and unoptimized crosslinking condictions, the resulting dielectric films prepared by spin-coating and post-annealing showed less than optimum surface morphologies (RMS roughness > 2 nm), compromising OFET performance, especially the mobility.

Furthermore, to enable deposition of the **CPB** films via roll-to-roll processes, it is of essential to control the crosslinking kinetics to avoid premature matrix condensation in solution before film deposition. Under this program we developed new α,ω–silane crosslinkers having tuned reactivity with respect to hydroxyl-containing polymers (**Figs. 12, 13**). An in situ kinetic study comparing the reactivity of chloro-, acetoxy-, dialkylamino-, and methoxysilanes with a hydroxylated reactant was performed, enabling a correlation of crosslinker-polymer reactivity with the corresponding **CPB** dielectric properties. With the new silane crosslinkers, we demonstrated that optimization of crosslinking conditions, especially by using moderately reactive crosslinking reagents (eg, C_6OAc), appropriate solvents, and polymer:crosslinker molar ratio, affords very low leakage and *very smooth* dielectric films. These new **CPB** formulations enable tunable thicknesses and capacitances, excellent leakage characteristics (**Fig. 13**), and can be fabricated on conventional Si substrates as well as on flexible Al/PEN and ITO/Mylar substrates via spin-coating or gravure printing. OFETs

Figure 13. Electrical properties of spin-coated thin **CPB** films fabricated with various crosslinkers (polymer:crosslinker ratios are as given in Table 2; C_6NMe_2 = blue, C_6Cl = black, C_6OAc = red, **EGOAc** = green). A. Leakage current density vs. voltage plot. B. Leakage current density vs. electric field plot. C. Capacitance-frequency plots ($1-10^3$ kHz) for ultra-thin (top) and thick (bottom) spin-coated **CPB** films. Abbreviations identified in Fig. 16.

fabricated with these new CPB dielectric films exhibit excellent performance.

3. Organic and Hybrid TFT Interfaces

Optimization of fabrication processes leading to high-quality interfaces between the TFT component materials, and understanding of what chemical, morphological, and microstructural phenomena best optimize charge flow in TFTs, is arguably as important as developing new materials. Thus, we devoted significant effort in this direction with success and key discoveries.

Gate Dielectric Viscoelasticity Effects on Transistor Response. Glassy polymer dielectrics are ideal candidates for OTFTs due to ease of processing from solution, printability, and mechanical flexibility. Since the charge carrier transport in OTFTs is confined to a very thin channel in the organic semiconductor (~ 2 – 9 nm, depending on the semiconductor) at the interface with the gate dielectric, it generally agreed that the physicochemical properties of the gate dielectric such
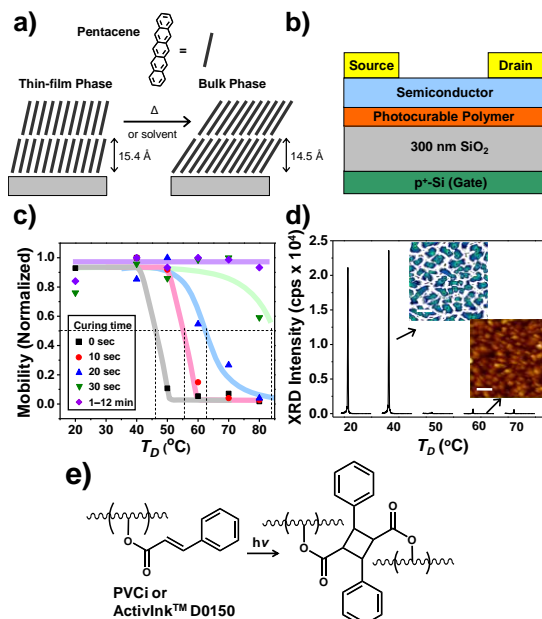
as surface roughness, chemical functionalization, and surface energy greatly affect the semiconductor film growth mode and microstructure, trapped charge density, and hence the corresponding OTFT device performance.

Under this program we first discovered that OTFT performance is substantially affected by the polymer gate dielectric viscoelasticity, i.e., the temperature-dependent segmental dynamics (motion) of the polymer chains (**Fig. 14**). A traditional observable of this property is the glass transition temperature of the bulk material [T_g(b)], which is the temperature at which the material passes from the glassy to the rubbery state. It is well-known that below a certain critical film thickness (h), the glass transition temperature
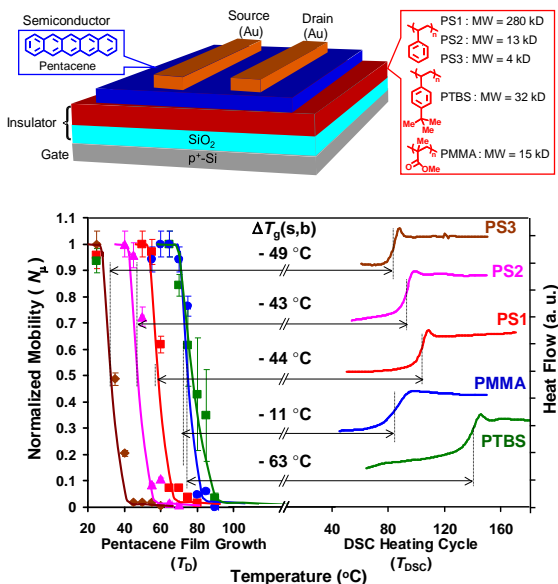
Figure 14. Top. Schematic representation of the top-contact, bottom-gate OTFT structure, and the materials components. **Bottom.** Normalized carrier mobility $N_\mu = \mu/\mu_{max}$ at different semionconductor deposition temperatures (T_Ds) for pentacene OTFTs on various bilayer insulators. Right: Differential scanning calorimetry (DSC) scans for the polymers investigated in this study. Herein the polymer surface glass transition temperature [T_g(s)] is defined as the temperature where $N_\mu = 0.5$, and ΔT_g (s,b) = T_g(s) − T_g(b).

Figure 15. a) Schematic of two pentacene polymorphs, the thin-film and bulk phase. b) Schematic of the top-contact/bottom-gate OTFT device geometry employed. c) Normalized field-effect mobility at the indicated T_Ds for pentacene TFTs on a crosslinkable D0150 dielectric with different curing times. d) XRD ($\theta/2\theta$ scans) data and AFM images (5 μm $\times$ 5 μm scan areas; scale bar = 1 μm) of 50 nm thick pentacene films grown on uncrosslinked D0150 at the indicated T_Ds. e) Crosslink chemistry for this dielectric.

of a film becomes thickness-dependent [defined as T_g(h)], being either lower or higher than T_g(b), depending on the interplay of the film free (top) and buried (bottom) interface vs. the bulk polymer chain dynamics. This behavior is relevant to fabricating organic electronic devices since they are usually composed of multi-stack thin films having many interfaces. Our initial results showed that gate dielectric polymer chain motion at temperatures well below T_g(b) and T_g(h) disturbs ordered semiconductor film growth on top of the dielectric film and compromises device performance. We empirically defined a TFT-derived glass transition temperature of the polymer film surface [T_g(s)] as the temperature at which the TFT carrier mobility decreases by 50 %. Besides technology aspects related to device fabrication, this discovery reveals that TFT measurements can be used to probe and differentiate the fundamental viscoelastic properties of the free surfaces from those of bulk and thin polymer films. We demonstrated that *$T_g(s)$ is*
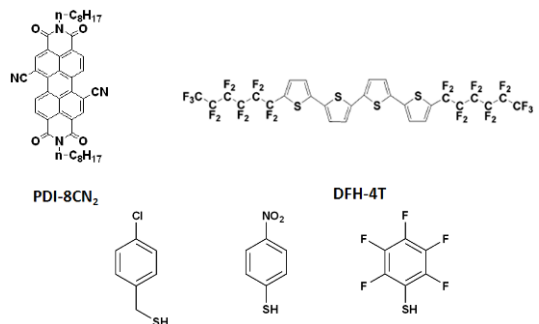
always lower than both $T_g(b)$ and $T_g(h)$ by using several polymeric dielectrics where the T_g(b) was systematically varied in chemical structure, molecular weight, and film thickness (**Fig. 14**).

The above findings raise the interesting question of what other polymer surface properties can be interrogated via TFT response. In crosslinked polymers, the introduction of crosslinks restricts chain segmental mobility and thus increases T_g(b). Furthermore, the degree of crosslinking in photocurable polymers can be fine-tuned, depending on the irradiation/curing time (t_c), and has often been evaluated by measuring T_g(b) and/or related polymer physical properties. More recently we demonstrated that organic TFTs can be used to probe the degree of crosslinking of dielectric polymer films and that fully crosslinked films are not required to maximize TFT response (**Fig. 15**). Furthermore, device performance variations can be clearly correlated with transitions of pentacene film morphology and microstructure.
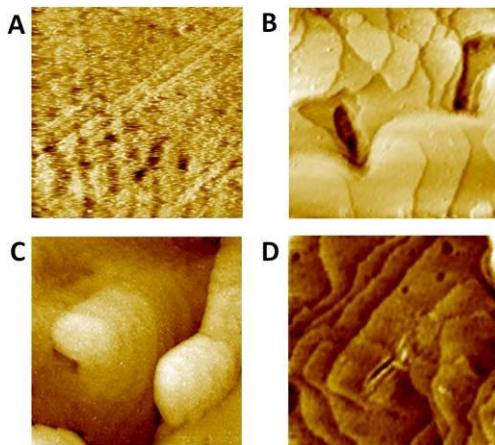
SAM Functionalization of Metal Contacts to Tune Charge Injection. The goal here is to understand how the morphological features of organic semiconducting films growing on bare and alkylthiol-functionalized metal contacts (**Fig. 16**), the typical materials used in coplanar (bottom-contact) TFT architectures, evolve on the nanoscale as film thickness increases from one monolayer to multilayers to typical OFET thicknesses. We seek correlations between film nanostructural features such as orientation, molecular alignment on metal contacts, the presence of structural defects, grain boundaries and other scattering centers, with OFET performance. In fact, the performance of bottom contact TFT structures lags behind that of top contact structures owing to severe contact resistance.

Figure 16. Semiconductors (top) and aromatic thiols (bottoms) used in these experiments.

The major sources of the contact resistance for bottom contact TFTs are believed to involve a combination of non-optimal semiconductor growth morphology on the contact surface and the limited available charge injection area versus top contact structures. As a part of an effort to understand the origin of high charge injection barriers in n-channel TFTs, we investigated the influence of thiol contact treatment on the molecular-level structures of such interfaces using hexamethyldisilazane (HMDS)-treated SiO_2 gate dielectrics. We focussed on contact surface treatment methods for TFTs based on two archetypal n-type semiconductors, α,ω-diperfluorohexylquarterthiophene (DFH-4T) and N,N' bis(*n*-octyl)-dicyanoperylene-3,4:9,10-bis(dicarb-oximide) (PDI-8CN$_2$) (**Fig. 16**). We find that TFT performance is remarkably enhanced on surface treatment--to the level of top contact device performance in terms of mobility, on/off ratio, and contact resistance. To analyze the molecule-level film structural

Figure 17. Dynamics of DFH-4T growth and evolution of the nanostructures in monolayer to multiplayer transition with and without thiol treatment of the Au(111) substrate. All STM images are in the 500 nm X 500 nm scan size. **A**. 3 nm DFH-4T on bare Au(111). **B.** 3 nm film of DFH-4T on thiol SAM/Au(111) substrate. **C.** 9 nm DFH-4T on bare Au(111) substrate. **D.** 9 nm DFH-4T on thiol SAM/Au(111) substrate.
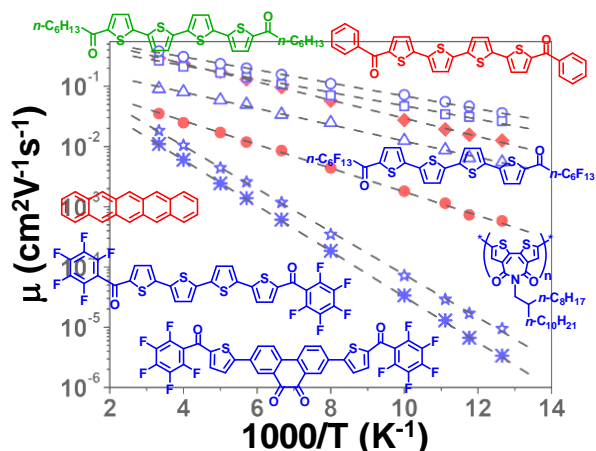
changes arising from the contact surface treatment, surface morphologies are characterized by AFM and STM. The high resolution STM images show that the growth orientation of the semiconductor molecules at the gold-semiconductor interface is maintained with the molecular long axes oriented along the SiO_2 surface normal (**Fig. 17**). As a result, the film microstructure is well-organized for charge transport in the interfacial region.

4. Charge Transport Investigations

In this section we show that under this AFOSR program, we were the first group to initiate detailed studies of charge transport mechanisms in n-type semiconductors as well as to correlate electron-transport with hole/ambipolar transport within a broad series of organic semiconductors.

Variable Temperature Mobility Analysis. The importance of understanding OTFT charge transport phenomena has been highlighted by recent discoveries. Separate studies argue that the ambient instability of n-channel FET operation for most organic semiconductors is the result of mobile electron trapping by ambient H_2O and/or O_2. These ideas were recently tested, refined, and implemented to develop intrinsically air-stable n-channel semiconductors not relying on an O_2 barrier. Further work demonstrated that rigorous exclusion of trapping species at the dielectric-semiconductor interface (e.g., hydroxyl groups) can enable n-channel TFT performance for both p-type and n-type semiconductors under inert atmosphere by

Figure 18. Chemical structures of the investigated p-channel (red), n-channel (blue), and ambipolar (green) semiconductors, and plots of TFT μ_{eff} vs. inverse temperature. The dashed lines are least-squares fits to the Arrhenius relationship.

eliminating deep electron traps with densities $> 10^{13}$ cm^{-2}. While these energetically deep, high-density charge traps must be overcome for efficient FET operation, it has been postulated that in most OFETs, shallow lower-density (~10^{10} cm^{-2} to ~10^{12} cm^{-2}) traps limit the effective mobility (μ_{eff}) for both p- and n-channel FET operation. Variable-temperature studies of TFTs have been used to characterize charge transport mechanisms, and generally reveal thermally-activated charge transport, with activation energies (E_As) on the order of 10's – 100's of meV. The most widely-accepted model for charge transport in polycrystalline organic semiconductors involves multiple trapping and release (MTR). This model postulates that free carrier mobility (μ_0) is diminished by recurrent charge carrier trapping and thermal release from shallow trap states below the conduction band edge, thereby defining the observed μ_{eff}. Since μ_{eff} is dominated by this trapping and release behavior, the density of these traps (N_{T0}, cm^{-2}) and their energy distribution in the band tail then determines the temperature dependence of μ_{eff}.

For the above reasons, we have begun to investigate the temperature dependence of TFT mobility for a series of n-channel, p-channel, and ambipolar organic semiconductor-based FETs selected for varied semiconductor structural and device characteristics (**Fig. 18**). Fits of the effective field-effect mobility (μ_{eff}) data assuming a discrete trap energy within a multiple trapping and release (MTR) model reveal low activation energies (E_As) for high-mobility semiconductors **1** - **3** of 21, 22 and 30 meV, respectively. Higher E_A values of 40 - 70 meV are exhibited by **4** – **7**-derived FETs having lower mobilities (μ_{eff}). Analysis of these data reveals

little correlation between the conduction state energy and E_A, while there is an inverse relationship between E_A and μ_{eff}. The first variable-temperature study of an ambipolar organic TFT reveals that although n-channel behavior exhibits $E_A = 27$ meV, the p-channel regime exhibits significantly more trapping with $E_A = 250$ meV. Interestingly, the calculated free carrier mobilities (μ_0) are in the range ~ 0.2 - 0.8 cm$^2$V^{-1}s^{-1} in this materials set, largely *independent* of μ_{eff} (**Fig. 19**). These results indicate that in the absence of charge traps, the inherent magnitude of carrier mobility is comparable for each of these materials. The effect of temperature on threshold voltage (V_T) was also analyzed and revealed two distinct trapping regimes, with the change in trapped charge exhibiting a
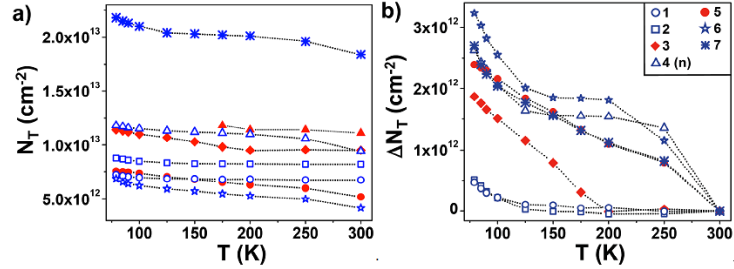
Figure 19. Plot of charge trap density (N_T) vs. temperature, calculated using the eq. $N_{SS}^{max} = \left[\dfrac{0.43429 \cdot S}{kT/q} \right] \dfrac{C_{ox}}{q}$ (**a**), and a plot of ΔN_T vs. temperature obtained from the eq $\Delta N_T = q\Delta V_T C_{ox}$ (**b**). The dotted lines in **a** and **b** are a drawn as a guide to the eye.

striking correlation with room temperature μ_{eff}. The observation that E_A is independent of conduction state energy, and that changes in trapped charge with temperature correlate with room temperature μ_{eff}, support the applicability of trap-limited mobility models such as a multiple trapping and release (MTR) mechanism to this materials set (**Fig. 19**).

Engineered Grain Boundaries for High-Performance and Reliable Solution-Processed Transistors. In this Task we used an n-channel semiconductor (PDI8-CN2; developed under AFOSR support) to fabricate organic transistors and to understand the role of the semiconductor film grain boundaries on performance (**Fig. 20**). In previous efforts we showed that solution-processed PDI8-CN2 TFTs exhibit large mobilities due to the formation of large grains. However, the desirable formation of large crystalline domains introduces grain boundaries, resulting in substantial device-to-device performance variations. Indeed, for films where the grain-boundary structure is random, a few unfavorable grain boundaries may dominate device performance. In this work we isolated the effects of molecular-level structure at grain boundaries by engineering the microstructure of PDI8–CN2 films, and analyzed their consequences for charge transport. A combination of synchrotron X-ray scattering, first-principles
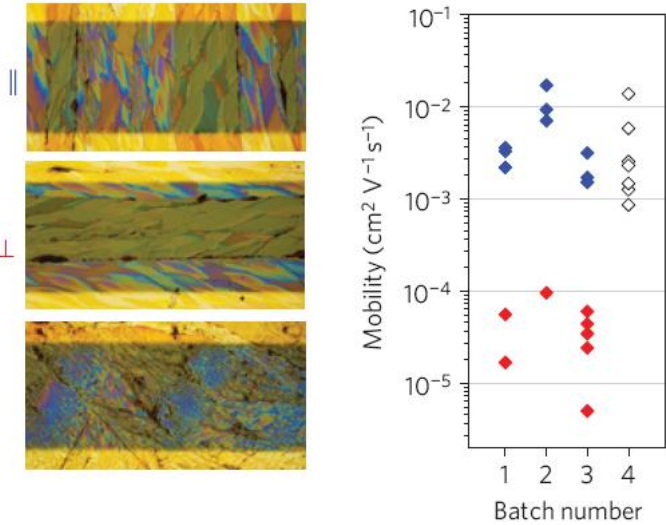
Figure 20. Mobility anisotropy for PDI8–CN2 films. Left: Optical micrographs of parallel (top), perpendicular (middle) and isotropic (bottom) TFTs fabricated from PDI8–CN2 films. Channel lengths are all 600 m. Right: Derived mobility of aligned and isotropic PDI8–CN2 films. In batch 1 devices were fabricated by evaporating top contacts on the active layer, whereas in batches 2, 3 and 4, films were grown on substrates with e-beam-deposited bottom contacts. Batch-to-batch variations are probably due to differences in device geometry and the time elapsed between substrate UV–ozone treatment and film growth, as this affects film quality.
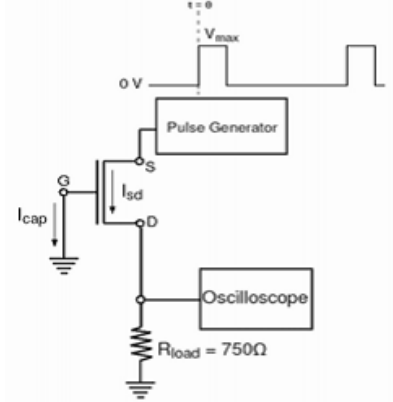
computation, and TFT characterization applied to PDI8–CN2 films reveals that grain-boundary orientation modulates carrier mobility by approximately 100x (**Fig. 20**). For PDI8–CN2, we showed that the molecular packing motif (that is, herringbone versus slip-stacked) plays a decisive role in grain-boundary-induced transport anisotropy. The results of this study provide important guidelines for designing molecular semiconductor-based optimized TFTs.

Dynamic Charge Transport Studies. Since **PDI8-CN$_2$** is currently the most promising n-type material, we began investigating in detail its charge transport dynamic response via transient measurements. Here, a bottom contact device with a channel width and length of 2000 μm and 7.5 μm, respectively, is employed. The device dielectric consisted of 1000 Å of SiO$_2$ under 2000 Å of Si$_3$N$_4$, with an estimated gate dielectric capacitance of 16.9 nF/cm^2. A film of about 400 Å of either pentacene (p-channel) or **PDI-8CN$_2$** was vacuum deposited at $<1 \times 10^{-7}$ Torr. All measurements were carried out under vacuum at 25°C. The circuit configuration used to measure the transient response is shown in **Fig. 21**. The OTFT gate is grounded, and a square wave from a voltage pulse generator is used to cycle the OTFT source between 0.0 V and a maximum positive voltage V_{max}, ranging from ~30 V - ~100 V in ~10 V increments .

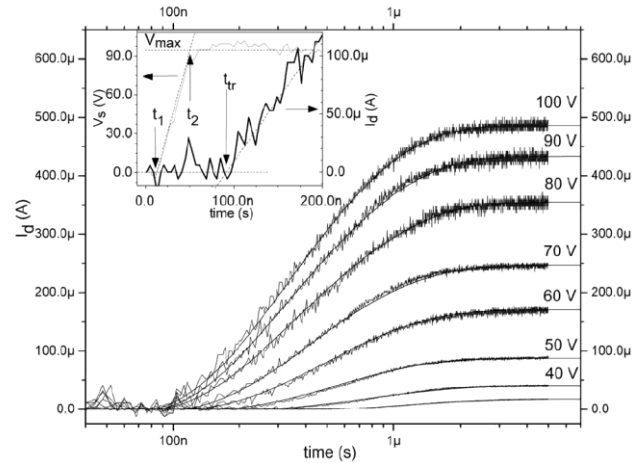

Figure 21. Circuit schematic for transit time measurements.

Fig. 22 shows the preliminary results. To estimate the mobility at ~100 ns, we used t_{tr}, the transit time of the fastest charges from the source to drain. On a linear scale (inset of **Fig. 26**), the voltage profile of the source voltage, V_s, may be approximated as a linearly increasing voltage signal from 0.0 V to some average saturation voltage, V_{max}, starting at time t_1 and ending at time t_2, after which it remains constant at V_{max}. Times t_1, t_2, and t_{tr} are shown in the inset of **Fig. 22**, which shows I_d and V_s for a

Figure 22. Transient response as a function of gate-source and drain-source voltage of a 7.5 μm channel length pentacene transistor. The inset depicts the times in eq. 3.

pentacene OFET at $V_{max} \approx 100$ V. Because t_{tr} is of the same order of magnitude as t_1 and t_2, the rise time of the source voltage must be taken into account in estimating μ from t_{tr}. We proceed by integrating the expression for velocity in terms of the mobility, $v = \mu V_s/L$, over the transit time and solving for μ:

$$\mu = \frac{L^2}{\frac{A}{2}\left[(t_2)^2 - (t_1)^2\right] + \left[V_{max}(t_{tr} - t_2)\right]}$$

(3)

where A is the slope of the voltage pulse between t_1 and t_2. The mobilities for each V_{max} are calculated using the values of V_{max}, A, t_1, t_2, and t_{tr} obtained as in the inset of **Fig. 23**, and are shown in **Fig. 23**. One explanation for the dependence of the mobility on V_s is that increasing

carrier density with increasing V_{sg} leads to a mobility saturation when the Fermi level of the charges in the channel rises sufficiently to fill all low-lying traps. The increasing lateral electric field in the channel is also a contributing factor. Data from **PDI8-CN₂** OTFTs are shown in **Fig. 23**. The data reveal a dependence of transit time on the source/drain field. These experiments clearly show that the drift mobility can be estimated through such experiments and compared to the field-effect mobility.
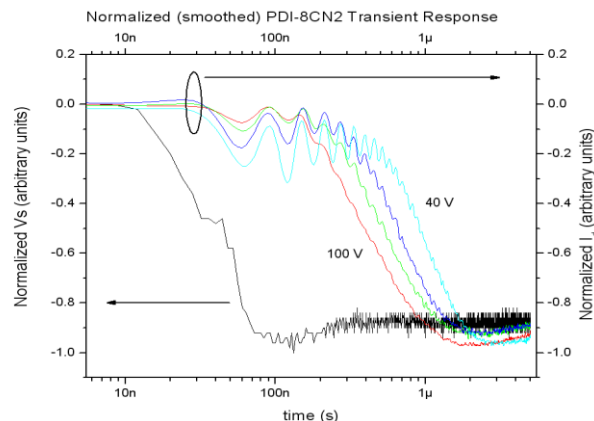
Figure 23. Transient response as a function of gate-source and drain-source voltage in a 7.5 μm channel length **PDI8-CN₂** TFT.

Publications Acknowledging Support by the AFOSR Program FA9550-08-1-0331

1. Ortiz, R. P.; Facchetti, A.; Marks, T. J. "High-k Organic, Inorganic, and Hybrid Dielectrics for Low-Voltage Organic Field-Effect Transistors" *Chem. Rev.* **2010**, *110*, 205-239.

2. Letizia, J. A.; Rivnay, J.; Facchetti, A.; Ratner, M. A.; Marks, T. J. "Variable Temperature Mobility Analysis of n-Channel, p-Channel, and Ambipolar Organic Field-Effect Transistors" *Adv. Funct. Mater.* **2010**, *20*, 50-58.

3. Dunn, L.; Dodabalapur, A. "Temperature dependent transient velocity and mobility studies in an organic field effect transistor" *J. Appl. Phys.* **2010**, *107*, 113714/1-113714/6.

4. Ortiz, R. P.; Yan, H.; Facchetti, A.; Marks, T. J. "Azine- and azole-functionalized oligo' and polythiophene semiconductors for organic thin-film transistors" *Materials* **2010**, *3*, 1533-1558.

5. Kim, C.; Quinn, J. R.; Facchetti, A.; Marks, T. J. "Pentacene Transistors Fabricated on Photocurable Polymer Gate Dielectrics: Tuning Surface Viscoelasticity and Device Response" *Adv. Mater.* **2010**, *22*, 342-346.

6. Zhan, X.; Facchetti, A.; Barlow, S.; Marks, T. J.; Ratner, M. A.; Wasielewski, M. R.; Marder, S. R. "Rylene and Related pi-Electron Diimides for Organic Electronics" *Adv. Mater.* **2011**, *23*, 268–284.

7. Anthony, J. E.; Facchetti, A.; Heeney, M.; Marder, S. R.; Zhan, X. "n-Type Organic Semiconductors in Organic Electronics " *Adv. Mater.* **2011**, *23*, 268-284.

8. Liu, J.; Buchholz, D. B.; Chang, R. P. H.; Facchetti, A.; Marks, T. J. "High-Performance Flexible Transparent Thin-Film Transistors Using a Hybrid Gate Dielectric and an Amorphous Zinc Indium Tin Oxide Channel" *Adv. Mater.* **2010**, 22, 2333-2337.

9. Marks, T.J. "Materials for Organic and Hybrid Inorganic/Organic Electronics," *MRS Bulletin*, **2010**, 35, 1018-1027.

10. Rivnay, J.; Jimison, L. H., Northrup, J. E.; Toney, M. F.; Noriega, R.; Lu, S.; Marks, T.J.; Facchetti. A.; Salleo, A. "Large modulation of carrier transport by grain-boundary molecular packing and microstructure in organic thin films" *Nature Mater.* **2009**, *8*(12), 952-958.

11. Kim, H.-S.; Won, S. M.; Ha, Y.-G.; Ahn, J.-H.; Facchetti, A.; Marks, T. J.; Rogers, J. A. "Self-assembled nanodielectrics and silicon nanomembranes for low voltage, flexible transistors, and logic gates on plastic substrates" *Appl. Phys. Lett.* **2009**, *95*(18), 183504/1-183504/3.

12. Kim, C.; Facchetti, A.; Marks, T. J. "Probing the Surface Glass Transition Temperature of Polymer Films via Organic Semiconductor Growth Mode, Microstructure, and Thin-Film Transistor Response" *J. Am. Chem. Soc.* **2009**, *131*, 9122-9132.

13. Facchetti, A.; Marks, T. J. "Self-assembled nanodielectrics (SANDs) for unconventional electronics" *Material Matters* **2009**, *4*(3), 64-67.

14. Kim, H.S.; Won, S. M.; Ha, Y.-G.; Ahn, J.-H.; Facchetti, A.; Marks, T. J.;Rogers, J. A. "Self-assembled nanodielectrics and silicon nanomembranes for low 2 voltage, flexible transistors, and logic gates on plastic substrates" *Appl. Phys. Lett.* **2009**, *95*(18), 183504/1-183504/3.

15. DiBenedetto, S. A.; Facchetti, A.; Ratner, M. A.; Marks, T. J. "Molecular Self-Assembled Monolayers and Multilayers for Organic and Unconventional Inorganic Thin-Film Transistor Applications" *Adv. Mater.* **2009**, *21*, 1407-1433.

16. Chen, P.-C.; Shen, G.; Chen, H.; Ha, Y.-G.; Wu, C.; Sukcharoenchoke, S.; Fu, Y.; Liu, J.; Facchetti, A.; Marks, T. J.; Thompson, M. E.; Zhou, C. "High-Performance Single-Crystalline Arsenic-Doped Indium Oxide Nanowires for Transparent Thin-Film Transistors and Active Matrix Organic Light-Emitting Diode Displays" *ACS Nano* **2009**, *3*, 3383-3390.

17. Ponce Ortiz, R.; Casado, J.; Hernandez, V.; Lopez Navarrete, J. T.; Letizia, J. A.; Ratner, M. A.; Facchetti,A.; Marks, T. J. "Thiophene-Diazine Molecular Semiconductors: Synthesis, Structural, Electrochemical, Optical, and Electronic Structural Properties; Implementation in Organic Field-Effect Transistors" *Chemistry* **2009**, *15*, 5023-5039.

18. Ha, Y.-G.; Facchetti, A.; Marks, T. J. "Push-Pull .pi.-Electron Phosphonic-Acid-Based Self-Assembled Multilayer Nanodielectrics Fabricated in Ambient for Organic Transistors" *Chem. Mater.* **2009**, *21*, 1173-1175.

19. Usta, H.; Risco, C.; Facchetti, A.; Ratner, M. A.; Marks, T. J. "Design, Synthesis, and Characterization of Ladder-Type Molecules and Polymers. Air-Stable, Solution-Processable n-Channel and Ambipolar Semiconductors for Thin-Film Transistors via Experiment and Theory."*J. Am. Chem. Soc.* **2009**, *131*, 5586-5608.

20. Jeong, Y. T.; Cobb, B. H.; Lewis, S. D.; Dodabalapur, A.; Lu, S.; Facchetti, A.; Marks, T. J. "Realization of dual-channel organic field-effect transistors and their applications to chemical sensing." *Appl. Phys. Lett.* **2008**, *93*, 133304/1-133304/3.

21.   Usta, H.; Facchetti, A.; Marks, T. J. "Synthesis and Characterization of Electron-Deficient and Highly Soluble (Bis)Indenofluorene Building Blocks for n-Type Semiconducting Polymers" *Org. Lett.* **2008**, *10*, 1385.

22.   Jones, B. A.; Facchetti, A. ; Wasielewski, M.I R.; Marks, T. J. "Effects of arylene diimide thin film growth conditions on n-channel OFET performance" *Adv. Funct. Mater.* **2008**, *18*, 1329-1339.

23.   Lu, G.; Usta, H.; Risco, C.; Wang, L.; Facchetti, A.; Ratner, M. A.; Marks, T. J. "Synthesis, Characterization, and Transistor Response of Semiconducting Silole Polymers with Substantial Hole Mobility and Air Stability. Experiment and Theory" *J. Am. Chem. Soc.* **2008**, *130*, 7670-7685.

24.   Jones, B. A.; Facchetti, A. ; Wasielewski, M. R.; Marks, T. J. "Tuning Orbital Energetics in Arylene Diimide Semiconductors. Materials Design for Ambient Stability of n-Type Charge Transport" *J. Am. Chem. Soc.* **2007**, *129*, 15259-15278.

25   Jones, B. A.; Facchetti, A.; Wasielewski, M. R.; Marks, T. J. "Effects of Arylene Diimide Thin Film Growth Conditions on n-Channel OFET Performance" *Adv. Funct. Mater.* **2007**, *18*, 1929-1939

26.   Kim, C.; Facchetti, A.; Marks, T. J. "Gate Dielectric Physicochemical Control of Pentacene Microstructure and Field-Effect Transistor Response" *Adv. Mater.* **2007**, *19*, 2561-2566.

27.   Lin, H. C; Kim, S. K.; Chang, D.; Xuan, Y.; Mohammadi, S.; Ye, P.; Gang, L.; Facchetti, A.; Marks, T. J. "Direct-current and radio-frequency characterization of GaAs metal-insulator-semiconductor field-effect transistors enabled by self-assembled nanodielectrics" *Appl. Phys. Lett.* **2007**, *91*, 092103.

28.   Yoo, B.; Jones, B. A.; Basu, D.; Fine, D.; Jung, T.; Mohapatra, S.; Facchetti, A. ; Dimmler, K.; Wasielewski, M. R.; Marks, T. J.; Dodabalapur, A. "High Performance Solution-Deposited n-Channel Organic Transistors and their Complementary Circuits" *Adv. Mater.* **2007**, *19*, 4028-4033.

29.   Jones, B. A.; Facchetti, A.; Marks, T. J.; Wasielewski, M. R. "Cyanonaphthalene Diimide Semiconductors for Air-Stable, Flexible, and Optically Transparent n-Channel Field-Effect Transistors" *Chem. Mater.* **2007**, *19*, 2703-2705.

Summaries of Student Theses Eminating from this Project (Full Theses Can be Obtained from Dissertation Abstracts).

1. Hakan Usta (Northwestern University)

π-Conjugated oligomeric and polymeric semiconductors have been the focus of intense research over the past few decades as alternatives to inorganic semiconductors for low-cost electronic applications such as organic field-effect transistors (OFETs). These materials enable vapor- or solution-phase fabrication of large-area, light-weight electronic devices, and are compatible with plastic substrates for mechanically flexible, conformable, and wearable electronics. Two primary challenges to realizing these applications are the ambient stability of organic thin films and solution-processability. Although several synthetic and device processing

strategies have led to air-stable semiconductors having charge mobilities ranging from 10^{-5} to $>$ 0.1 cm^2/V·s, there are still very few *p*-type polymeric and n-type or ambipolar molecular/polymeric semiconductors exhibiting truly high performance (charge mobility $\geq$ 0.1 cm^2/V·s, I_{on}/I_{off} ratio of $>10^5$). Thus, the development of new solution-processable, π-conjugated semiconductors exhibiting high field-effect carrier mobility and good stability under ambient conditions is of great interest. Furthermore, the fundamentals governing device environmental stability and FET performance with respect to the molecular/polymeric structure should be understood in greater depth.

This study addresses these challenges via theory-aided rational design, synthesis, and characterization of novel hole- and electron transporting molecules and polymers as air-stable and solution-processable semiconductors for high performance *p*-channel, *n*-channel, and ambipolar OFETs. Significant correlations are established between molecular/polymeric structures, physicochemical properties, and OFET device performance, providing detailed insight into charge transport characteristics and ambient stability. In the first part, a series of dibenzosilole- and dithienosilole-based homo- and copolymers were developed for air-stable solution-cast *p*-channel FETs with high hole mobilities up to 0.08 cm^2/V·s and current modulations of $10^5 - 10^6$. In the second part, a new family of carbonyl-/dicyanovinylene-functionalized bis(indenofluorene) compounds and their corresponding homo- and copolymers were synthesized and characterized. Thin films of these semiconductors yield OFETs with high electron mobility (up to 0.16 cm^2/V·s) and high I_{on}/I_{off} ratio ($10^7 - 10^8$), one of the highest to date for a solution-cast air-stable *n*-channel semiconductor. Additionally, we reported the first examples of polymeric and molecular ambipolar semiconductors to function in air. Detailed analysis of the operational air-stabilities of a series of thin-films shows that air stability is principally governed by LUMO energetics with minimal contribution from thin film microstructure. The onset LUMO energy for carrier electron stabilization is estimated as -4.1 – -4.0 eV. Density functional theory calculations provide detailed insight into molecule/polymer physicochemical and charge transport characteristics. These results, in total, affirm the possibility of achieving low-cost microelectronic devices through organic materials that enable simple solution fabrication processes under ambient conditions.

2. Choongik Kim (Northwestern University)

Organic thin-film transistors (OTFTs) have been extensively studied for organic electronics. In these devices, organic semiconductor-dielectric interface characteristics play a critical role in influencing OTFT operation and performance. This study begins with exploring how the physicochemical characteristics of the polymer gate dielectric affects the thin-film growth mode, microstructure, and OTFT performance parameters of pentacene films deposited on bilayer polymer (top)-SiO$_2$ (bottom) dielectrics. Pentacene growth mode varies considerably with dielectric substrate, and correlations are established between pentacene film deposition temperature, the thin-film to bulk microstructural phase transition, and OTFT device performance. Furthermore, the primary influence of the polymer dielectric layer glass transition temperature on pentacene film microstructure and OTFT response is shown for the first time.

Following the first study, the influence of the polymer gate dielectric viscoelastic properties on overlying organic semiconductor film growth, film microstructure, and TFT response are investigated in detail. From the knowledge that nanoscopically-confined thin polymer films exhibit glass transition temperatures that deviate substantially from those of the

corresponding bulk materials, pentacene (p-channel) and cyanoperylene (n-channel) films grown on polymer gate dielectrics at temperatures well-below their bulk glass transition temperatures (T_g(b)) have been shown to exhibit morphological/microstructural transitions and dramatic OTFT performance discontinuities at well-defined temperatures (defined as the polymer "surface glass transition temperature," or T_g (s)). These transitions are characteristic of the particular polymer architecture and independent of film thickness or overall film cooperative chain dynamics. Furthermore, by analyzing the pentacene films grown on UV-curable polymer dielectrics with different curing times (hence, different degrees of crosslinking), clear correlations between pentacene film deposition temperature, degree of polymer dielectric film crosslinking, and the corresponding pentacene film growth mode, phase composition, and carrier mobilities are established. Based on the results, TFT measurements have been demonstrated to represent a new and sensitive methodology to probe polymer surface viscoelastic properties as well as the degree of polymer dielectric film crosslinking.

In the final study, the synthesis and dielectric properties of optimized crosslinked polymer blend (CPB) dielectrics for printable TFTs are reported. Novel silane crosslinking reagents with tuned reactivity enable the fabrication of CPB films having excellent quality and tunable thickness, fabricated both by spin-coating and gravure-printing. The CPB dielectric films fabricated by blending crosslinking reagent with poly(4-vinyl)phenol (PVP) require very low-curing temperatures (~110 $^{\circ}$C), tenaciously adhere to a variety of TFT gate contact materials and exhibit excellent insulating properties with tunable capacitance values. The CPB film quality is correlated with the PVP-crosslinking reagent reactivity. Devices fabricated with both p- and n-channel organic semiconductors on the CPB dielectrics function at low operating voltages and the device performance is strongly correlated with the morphology and microstructure of the representative semiconductor films.

3. **Young-Geun Ha (Northwestern University)**

Organic thin-film transistors (OTFTs) have been the focus of intense research over the past few decades as alternatives to silicone-based conventional transistors. In these devices, dielectric characteristics play a critical role in influencing OTFT operation and performance. My thesis research focuses on two novel classes of dielectric materials based on organic-inorganic hybrid blends and hybrid multilayers. At first, the design, synthesis, processing, and dielectric properties of novel crosslinked inorganic/organic hybrid blend (CHB) dielectric films for low-voltage organic thin film transistor (OTFT) operation are introduced. CHB thin films are readily fabricated by spin-coating a zirconium chloride precursor + an α,ω-disilylalkane crosslinker solution in ambient, followed by curing at low temperatures (~150 °C). The very smooth CHB dielectrics exhibit excellent insulating properties (leakage current densities ~ 10^{-7} A/cm^2), tunable capacitance (95 − 365 nF/cm^2), and high dielectric constants (5.0 − 10.2). OTFTs fabricated with pentacene and PDIIF-CN$_2$ as the organic semiconductor function well at low voltages (< -4.0 V). The morphologies and microstructures of representative pentacene films grown on CHB dielectrics prepared with incrementally varied compositions and processing conditions are investigated and shown to correlate closely with OTFT response. Furthermore, pentacene OTFTs fabricated on plastic substrates with these new hybrid dielectrics are shown to operate at low voltages (< -4.0 V), and to offer high on-off current ratios (>10^5) as well as substantial hole mobilities (0.2-1.5 cm^{2}V^{-1}s^{-1}).

Secondly, the rational synthesis, processing, and dielectric properties of novel layer-by-layer organic/inorganic hybrid multilayer dielectric films are introduced. These new zirconia-based self-assembled nanodielectric (Zr-SAND) films (5 ~12 nm thick) are readily fabricated via solution processes under ambient atmosphere using polarizable π-electron phosphonic acid building blocks and ultra-thin ZrO_2 layers. Attractive Zr-SAND properties include amenability to accurate control of film thickness, large-area uniformity, well-defined nanostructure, exceptionally large electrical capacitance (up to 750 nF·cm^{-2}), excellent insulating properties (leakage current densities as low as 10^{-7} A·cm^{-2}), and excellent thermal stability. Thin-film transistors (TFTs) fabricated with pentacene and PDIF-CN_2 as representative organic semiconductors and zinc-tin-oxide (Zn-Sn-O) as a representative inorganic semiconductor, function well at low voltages (< ± 4.0 V). Furthermore, the TFT performance parameters of representative organic semiconductors deposited on Zr-SAND films, functionalized on the surface with various alkylphosphonic acid self-assembled monolayers, are investigated and shown to correlate closely with the alkylphosphonic acid chain dimensions.

4. **Joseph Letizia (Northwestern University)**

Electron transporting (n-channel) polymer semiconductors for field effect transistors are rare. In this investigation, the synthesis and characterization of new electron-depleted *N*-alkyl-2,2'-bithiophene-3,3'-dicarboximide-based π-conjugated homopolymers and copolymers containing the 2,2'-bithiophene unit are reported. A novel design approach is employed using computational modeling to identify favorable monomer properties such as core planarity, solubilizing substituent tailorability, and appropriate electron affinity with gratifying results. Monomeric model compounds are synthesized to confirm these properties, and a crystal structure reveals a short 3.43 Å π-π stacking distance with favorable solubilizing substituent orientations. A family of ten homopolymers and bithiophene copolymers is then synthesized via Yamamoto and Stille polymerizations, respectively. Two of these polymers are processable in common organic solvents: the homopolymer poly(*N*-(2-octyldodecyl)-2,2'-bithiophene-3,3'-dicarboximide) (**P1**) exhibits n-channel FET activity, and the copolymer poly(*N*-(2-octyldodecyl)-2,2':5',2'':5'',2'''-quaterthiophene-3,3'-dicarboximide) (**P2**) exhibits air-stable p-channel FET operation. After annealing, **P1** films exhibit a very high degree of crystallinity and an electron mobility > 0.01 $cm^2V^{-1}s^{-1}$ with a current on-off ratio of 10^7, which is remarkably independent of film-deposition conditions. Extraordinarily, **P1** films also exhibit terracing in AFM images with a step height matching the X-ray diffraction d-spacing, a rare phenomena for polymeric organic semiconductors. Another fascinating property of these materials is the air-stable p-channel FET performance of annealed **P2** films, which exhibit a hole mobility of ~0.01 $cm^2V^{-1}s^{-1}$ and a current on-off ratio of 10^7.

Temperature-activated field-effect transistor (FET) mobility is analyzed for a series of n-channel, p-channel, and ambipolar organic semiconductor-based FETs selected for varied semiconductor molecular and device characteristics. The materials (and dominant carrier type) studied are: 5,5'''-bis(perfluorophenacyl)-2,2':5',2'':5'',2'''-quaterthiophene (**1**, n-channel); 5,5'''-bis(perfluorohexyl carbonyl)-2,2':5',2'':5'',2'''-quaterthiophene (**2**, n-channel); pentacene (**3**, p-channel); 5,5'''-bis(hexylcarbonyl)-2,2':5',2'':5'',2'''-quaterthiophene (**4**, ambipolar); 5,5'''-bis(phenacyl)-2,2': 5',2'':5'',2'''-quaterthiophene (**5**, p-channel); 2,7-bis((5-perfluorophenacyl)thiophen-2-yl)-9,10-phenanthrenequinone (**6**, n-channel); and poly(*N*-(2-octyldodecyl)-2,2'-bithiophene-3,3'-dicarboximide) (**7**, n-channel). Fits of effective field-effect

mobility (m_{eff}) data assuming a discrete trap energy within a multiple trapping and release (MTR) model reveal low activation energies (E_As) for high-mobility semiconductors **1** - **3** of 21, 22 and 30 meV, respectively. Higher E_A values of 40 - 70 meV are exhibited by **4** – **7**-derived FETs having lower mobilities (m_{eff}). Analysis of these data reveals little correlation between the conduction state energy level and E_A, while there is an inverse relationship between E_A and m_{eff}. The first variable-temperature study of an ambipolar organic FET reveals that although n-channel behavior exhibits E_A = 27 meV, the p-channel regime exhibits significantly more trapping with E_A = 250 meV. Interestingly, calculated free carrier mobilities (m_0) are in the range ~ 0.2 - ~ 0.8 $cm^2V^{-1}s^{-1}$ in this materials set, largely independent of m_{eff}. This indicates that in the absence of charge traps, the inherent magnitude of carrier mobility is comparable for each of these materials. Finally, the effect of temperature on threshold voltage (V_T) reveals two distinct trapping regimes, with the change in trapped charge exhibiting a striking correlation with room temperature m_{eff}. The observation that E_A is independent of conduction state energy, and that changes in trapped charge with temperature correlate with room temperature m_{eff}, support the applicability of trap-limited mobility models such as a multiple trapping and release (MTR) mechanism to this materials set.

5. **Brian Cobb (University of Texas)**

The charge transport mechanisms in a solution-processable n-channel organic thin film transistor (OTFT), based on conjugated polymer, are thoroughly investigated. Temperature dependent steady state characteristics are studied to extract the trap density of states (DOS). Transport in the non-quasistatic or transient regime is investigated and the dynamic mobility and the velocity distribution of charge carriers in the channel. Transport parameters extracted from transient measurements correlate well with those obtained from steady state measurements. These studies included the temperature-dependent dynamic and steady-state response of an electron channel organic field effect transistor fabricated using *N,N'-n*-octyl dicyanoperylenediimide (PDI-8CN$_2$).   By measuring the time required for the device to turn on, the dynamic carrier mobilities for the fastest carriers, and the corresponding activation energies as well as the distribution of velocities can be extracted. Consistently higher dynamic mobilities and consistently lower dynamic activation energies are found compared to values obtain from quasi steady-state (DC) measurements.   These results were discussed in the context of the density of states of the material.